ChemBioChem

Research Article
doi.org/10.1002/cbic.202200423

Chemistry
Europe
European Chemical
Societies Publishing

www.chembiochem.org

Prebiotic Foam Environments to Oligomerize and Accumulate RNA

Emre Tekin,[a] Annalena Salditt,[a] Philipp Schwintek,[a] Sreekar Wunnava,[a] Juliette Langlais,[a] James Saenz,[b] Dora Tang,[c] Petra Schwille,[d] Christof Mast,[a] and Dieter Braun*[a]

When water interacts with porous rocks, its wetting and surface tension properties create air bubbles in large number. To probe their relevance as a setting for the emergence of life, we microfluidically created foams that were stabilized with lipids. A persistent non-equilibrium setting was provided by a thermal gradient. The foam's large surface area triggers capillary flows and wet-dry reactions that accumulate, aggregate and oligomerize RNA, offering a compelling habitat for RNA-based early life as it offers both wet and dry conditions in direct neighborhood. Lipids were screened to stabilize the foams. The prebiotically more probable myristic acid stabilized foams over many hours. The capillary flow created by the evaporation at the water-air interface provided an attractive force for molecule localization and selection for molecule size. For example, self-binding oligonucleotide sequences accumulated and formed micrometer-sized aggregates which were shuttled between gas bubbles. The wet-dry cycles at the foam bubble interfaces triggered a non-enzymatic RNA oligomerization from 2′,3′-cyclic CMP and GMP which despite the small dry reaction volume was superior to the corresponding dry reaction. The found characteristics make heated foams an interesting, localized setting for early molecular evolution.

Introduction

The emergence of Darwinian evolution demands that already the earliest form of life must be capable of *replication* and *mutation* to then be *selected* by its environment in order to adapt and develop further.[1] A candidate for life's first polymer is proposed by the RNA world hypothesis.[2] RNA can store information and fold into catalytic structures, also known as ribozymes. A ribozyme replicator could therefore have been a suitable starting point for molecular evolution and could have predated the otherwise necessary simultaneous emergence of functional proteins and DNA as information storage.[3]

[a] E. Tekin, A. Salditt, P. Schwintek, S. Wunnava, J. Langlais, Dr. C. Mast,
    Prof. Dr. D. Braun
    Systems Biophysics
    Center for Nano-Science and
    Origins Cluster Initiative Department of Physics
    Ludwig-Maximilians-Universität München
    Amalienstrasse 54, 80799 München (Germany)
    E-mail: dieter.braun@lmu.de
[b] Dr. J. Saenz
    Center for Molecular Bioengineering
    Technische Universität Dresden
    Helmholtzstrasse 10, 01069 Dresden (Germany)
[c] Dr. D. Tang
    Dynamic Protocellular Systems
    Max-Planck Institute for Molecular Cell Biology and Genetics
    Pfotenhauerstrasse 108, 01307 Dresden (Germany)
[d] Prof. Dr. P. Schwille
    Cellular and Molecular Biophysics
    Max-Planck Institute of Biochemistry
    Am Klopferspitz 18, 82152 Martinsried (Germany)

For entropic reasons, the prebiotic synthesis of RNA polymers from monomers had to be driven by non-equilibrium boundary conditions, such as temperature, pH or salt gradients. On the early earth, for example, hydrothermal vents or springs, volcanic eruption sites or heated ponds would offer temperature gradients at various scales. For replication to keep sequence information despite various degradation channels, a local reduction of entropy would be a central pre-requisite for Darwinian processes,[4] notably enhancing the concentration of the participating molecules against diffusion. One example of such a recently discussed scenario is the convection of water in pores of heated volcanic rocks.[5] Such thermal gradients were a likely setting at early earths hot crust[6] and were shown to drive polymerase-based DNA replication towards increasing length.[7]

Various studies have been recently published on the role of thermal gradient systems for the emergence of life. For example, a pointed heat source led to highly efficient RNA-catalyzed amplification of short RNA,[8] the circulation of lipid vesicles in a thermal gradient gave rise to fission by membrane-phase transitions[9] or by cycling temperatures of a random pool of 12 nucleotide long DNA, selective oligomer structures emerged by templated ligation.[10] Within this context, gas-water interfaces were discussed, as they drive a continuous enrichment of molecular structures under a temperature gradient.[5] Morasch *et al.* focused on the effects of gas-water interfaces, that were created with the help of single gas-filled cavities surrounded by a liquid. Here, we introduced foam into the reaction compartments and could significantly increase the interfacial area. Also, the addition of prebiotic more probable surfactants created additional structures at the interfaces.

Foams are heterogeneous inclusions of gas in liquids stabilized by surface active reactants, i.e., surfactants. Their very high surface to volume ratio promotes phase boundary processes such as gelation, accumulation and phosphorylation.

ChemBioChem

Research Article
doi.org/10.1002/cbic.202200423

Chemistry
Europe
European Chemical
Societies Publishing

Shallow hydro-thermal and volcanic settings may have led to ascending gas that passed through numerous porous rocks and formed micro scale foam environments. Alkaline hydrothermal vents are hypothesized to be a favorable environment for the emergence of the first protocell.[11] Studies have shown that in hydro-thermal fields (e.g. in Mount Lassen, California), myristic acid added to warm spring water gave rise to the self-assembly of foams and membranous compartments.[12]

We base this study on 2′,3′-cyclic mononucleotides (cNMP) which (a) possess an intrinsically activated phosphate; (b) are products of several prebiotic phosphorylation and nucleotide syntheses[13–17] and (c) are products of neutral to alkaline chemical and enzymatic hydrolyses of RNA.[18–22] In comparison, the dry polymerization of 3′,5′-cGMP[23–25] did not foster the polymerization of the other ribonucleotides.[25] Orgel and coworkers, reported conditions for 2′,3′ cAMP polymerization by drying for 40 days with a 5-fold excess of ethane 1,2 diamine and yields up to 0.67 % of 14-mers.[26,27] Other catalysts such as imidazole or urea required temperatures up to 85 °C and offered lower yields.
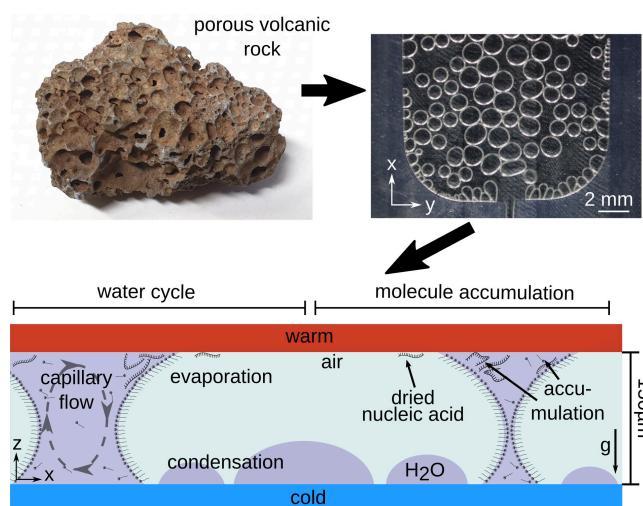
In a highly diluted, hadean ocean, around 4.4 billion years ago,[28] environments that promote high concentrations were crucial for triggering polymerization and fast reactions kinetics. Moreover, the localization of reaction products is deemed central for evolution to proceed. In this work, we showed that foams, in comparison to environments with low surface to bulk ratio, could improve the yield of reactions by the presence of heated gas-water interfaces. A non-enzymatic polymerization reaction was examined in both environments and produced significantly higher yield for the polymerization of RNA.
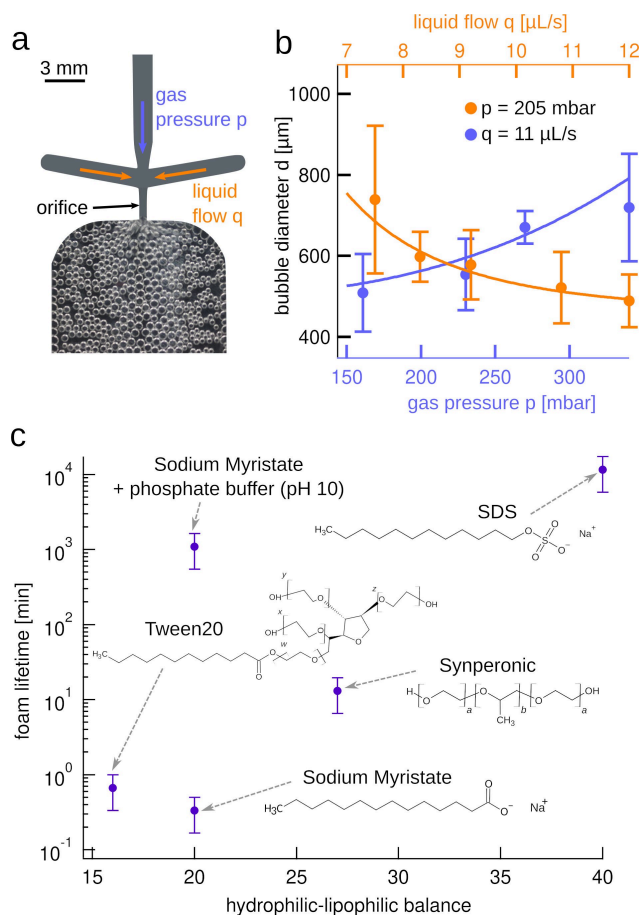

Figure 1. Foam in heated rock pores. Gas bubbles in heated porous volcanic rocks enable a prebiotic scenario of microfluidic foam systems, triggered by a thermal gradient. The scenario was recreated by foam filled 150 μm thick FEP cut-outs between heated sapphires. The surfactant solution of super-saturated sodium myristate created large foam structures as the surfactant adsorbed at gas-water interfaces and stabilized the gas bubbles. A temperature gradient triggered a continuous water cycling by evaporative capillary flow at the bubble interface of the foam that accumulated nucleotides at the warm side of the foam bubbles (grey arrow). The water vapor recondensed at the cold side and was shuttled by bubble aggregation driven by the surface tension back into the solution. This release of condensed water droplets into the bulk solution caused the gas bubble to fluctuate in size, transporting the dry accumulated nucleotides back into solution, establishing a localized, continuous wet-dry cycle similar to a heated air-water interface.[5]

Results and Discussion

Foam creation

In order to create reproducible and prebiotically more probable foam environments, we imitated micrometer sized pores and cracks in rocks with the help of shaped FEP foils clamped between two sapphires. These 150 μm–500 μm thick chambers can be filled with liquid and gas, temperature gradients can be applied, and fluorescent as well as bright light microscopy readout is possible. Figure 1 shows a schematic sketch of the cross-section of a surfactant stabilized bubble in a thermal gradient. Inside the gas bubble water evaporates at the warm side and condenses at the cold side, forming pure water droplets.

For foam fabrication by the co-flow method, a controlled supply of surfactant solution (e.g., 1.5 mM - 4 mM SDS or Tween20) and gas pressure was required. The surfactant solution flowed in from two opposite channels and periodically pinched off gas coming in from the mid channel (Figure 2a). The gas pressure and liquid flow could be varied from 180 mbar to 400 mbar and 10 μLs^{-1} to 40 μLs^{-1}, which allowed for control over the average bubble sizes. Similar to other publications[29,30] that studied micro fluidic foams, we found d~p and d~q^{-1},

with the bubble diameter d, gas pressure p and liquid flow q (Figure 2b). As pressure increased and flow decreased, the bubble sizes grew. Likely, due to its chemical structure and resulting packaging shape sodium myristate did not allow for precise control over the average bubble size, contrary to Tween20 or SDS.

We tested several lipids to create stable foams under the thermal gradient. In Figure 2c we plot the tested lipids' foam lifetimes over five orders of magnitude and plotted it against their corresponding hydrophilic lipophilic balance values. The lifetime was defined by the time half of the initial bubbles vanished in a 150 μm thick chamber while being exposed to a thermal gradient of $\Delta T = T_{warm} - T_{cold} = 62 °C – 25 °C = 37$ K.

For the ion induced stabilization of the foam in temperature gradients we used 200 mM dipotassium phosphate buffer. Phosphorus is a vital component of life, as it is essential for phosphorylation reactions for RNA and phospholipids. Carbonate-rich lakes can concentrate phosphorus up to more than 1 M.[34] Due to the prebiotic plausibility and long lifetime a mixture of ~3.2 mM supersaturated sodium myristate and 200 mM dipotassium phosphate buffer was used for further experiments.

Fatty acids, such as myristic acid, can be synthesized under prebiotically more probable conditions[31,32] and are therefore considered reasonable candidates for our foam experiments. We found that charged fatty acids are well suited for foam fabrication as their solubility is higher compared to their

ChemBioChem

Research Article
doi.org/10.1002/cbic.202200423

Chemistry Europe
European Chemical
Societies Publishing

Figure 2. Foam formation and lifetime. a) Foam was generated in a micro-fluidic setup using the co-flow method. Gas pressure was applied to the central channel (purple arrow). The lateral inflow of the surfactant solution (orange arrows) allowed the pinch off of gas bubbles, so that the chamber was filled with foam within approximately 4 seconds. b) Tuning the liquid flow q and the gas pressure p allowed to control the average bubble diameter d. The shown foam was created using a 4.5 mM Tween20 solution. Data for a constant pressure of $p = 205$ mbar by varying flow and a constant flow of $q = 11$ μLs^{-1} per channel by varying pressure is plotted. We found an approximate proportionality $d \sim p$ and $d \sim q^{-1}$. As a guide to the eye, power functions of the form $d(x) = k_0{}^* \times k1 + k_2$ were displayed. The error bars represent the standard deviation from the average bubble diameter. c) The choice of surfactant influenced the lifetime of the corresponding foam in a thermal gradient of $\Delta T = 37$ K across the 150 μm thick chamber. Surfactants with a high hydrophilic-lipophilic balance tended to increase the life span of the foam. The addition of 200 mM dipotassium phosphate buffer to the supersaturated sodium myristate solution drastically increased the lifetime from several seconds to 20.5 h. The error bars were estimated to be 50 % (see Figure S10).

uncharged counterparts. In addition, the lifetime of sodium myristate increased significantly when the solution was enriched with ions. The likely reason is that the addition of ions to the surfactant solution shields the headgroup repulsion of the lipid, which enables better packing at the interface.[33] Consequently, the critical packaging shape improves, and bubble formation is enhanced.

Accumulation of nucleotides

After having established a reproducible and stable way to form foams from prebiotically more probable surfactants, we investigated how the foams accumulate oligonucleotides. We prepared a solution of 3.2 mM sodium myristate, 200 mM dipotassium phosphate buffer and 10 μM Cy5 labeled, 14 nucleotide long ssDNA as a fluorescently marked proxy for polymerized RNA (see Supporting Information Table S1 for details). We have established previously, that DNA and RNA in capillary flow driven air-water systems behave similarly.[10]
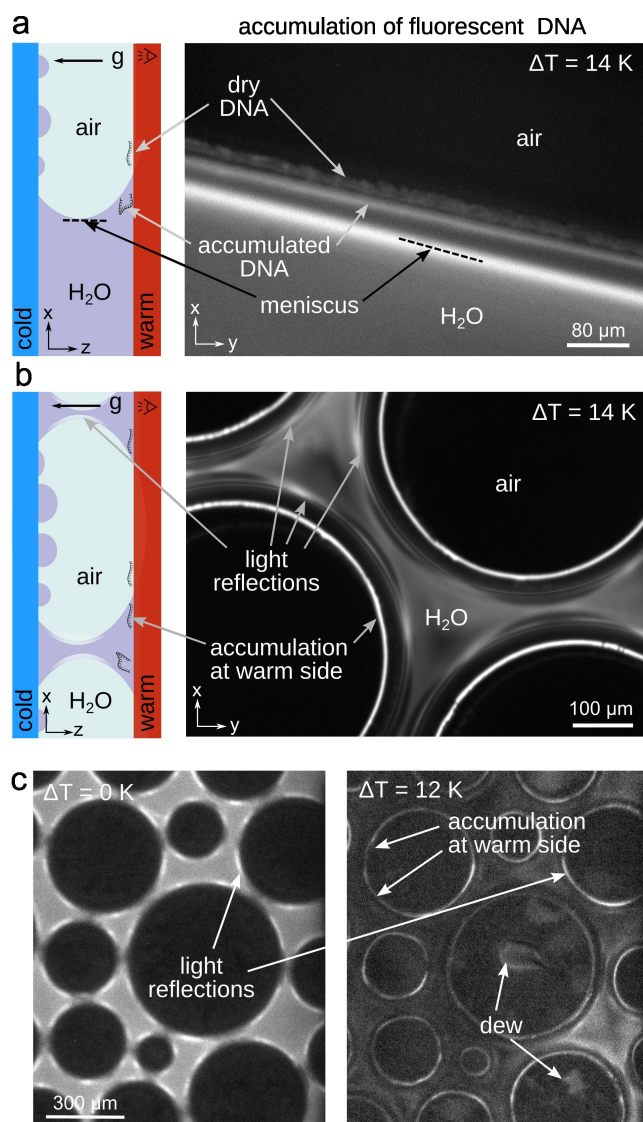
To compare the behavior of the DNA in a high surface area system (foam) and at a low surface areas system (single gas-water interface), a thermal gradient was applied to each system (Figure 3a, b). In both systems the same solution was injected, so that the only difference was the surface area. into the second chamber in the form of foam. The injection process of foam and sample is described in the Supporting Information (Figure S8). When the 150 μm thick chambers were exposed to a thermal gradient (here, $\Delta T = T_{warm} - T_{cold} = 52\,°C - 38\,°C = 14$ K), similar wet-dry dynamics and liquid fluxes occurred at the gas-water interfaces of both systems.

In both systems, evaporation at the warm side triggered capillary flows and accumulated molecules at the warm side of the water-gas interface, accumulating DNA.[5] The gaseous water is recondensed at the cold side either into the bulk or in form of dew droplets either at the open interface or inside the air-filled bubbles of the foam. They are invisible in the fluorescence images of Figure 3 since they consist of pure water without fluorescence molecules. Close to the interface, the pure droplets went back to solution by surface tension and temporarily reduced local ion and molecule concentrations, which is analogous to "rainfall" in the macroscopic water cycle.[35] The constant water cycle induced a fluctuating water level in the low surface area system, but in foam it led to fluctuation of the gas bubble diameters (Figure S11). In both cases, the fluctuating gas-water interfaces captured the accumulated molecules in continuous wet-dry cycles.

During the buildup of the thermal gradient an initial phase of Ostwald ripening[36] was found and spontaneous degassing led to small bubbles of the foam disappearing in favor of larger bubbles (see Movie S2). When the buildup of the thermal gradient equilibrated, only much fewer bubbles collapsed and created larger gas bubbles. These effects caused slight movement of gas bubbles. Molecules that were captured in wet-dry cycles at the interfaces were torn out of the continuous cycle and left in the dry as the contact line between air and water receded away from them.

In Figure 3c, the accumulation and distribution of DNA is shown before and after the application of a thermal gradient of $\Delta T = T_{warm} - T_{cold} = 49\,°C - 37\,°C = 12$ K in z-direction. Due to the temperature dependence of the surface tension, the thermal gradient contracted the bubble at the warm side and expanded it at the cold side, which induced rather a truncated cone-like structure of the bubble. The top view through the sapphire gave a picture, in which two nested rings were observed, similar to Figure 3b. The bright inner ring of accumulated material was

ChemBioChem

Research Article
doi.org/10.1002/cbic.202200423

**Chemistry
Europe**
European Chemical
Societies Publishing

Figure 3. Capillary flow accumulates oligonucleotides at a gas-water interface and inside foams. a) Cross-section of a heated chamber filled with water and gas next to a fluorescent image of 14 nucleotide long FAM-labelled DNA at a single gas-water interface. DNA accumulated at the interface and eventually dried out. Oscillating water levels inside the foam bubbles redissolved the dried DNA and evoked a wet-dry cycle. Surface tension and temperature differences lead to a meniscus shaped interface, that produced two bright fluorescent lines with accumulated DNA. The sample was exposed to a temperature gradient of $\Delta T = T_{warm} - T_{cold} = 52\,°C - 38\,°C = 14\,K$. b) Around the gas bubbles of the foam we found ring formed accumulations of DNA due to the capillary flow of evaporating water on the warm side. At the bubble surfaces light reflections appear, which are not to be confused with the direct fluorescence signal of concentrated DNA. c) Fluorescence image of foam before and after the application of a thermal gradient of $\Delta T = T_{warm} - T_{cold} = 49\,°C - 37\,°C = 12\,K$. Water cycles inside the gas bubbles lead to luminous spots, which originated from growing dew droplets that spread from the cold to the warm side and thus rehydrating dry material inside the gas bubbles. Light reflexes can be distinguished from accumulation, as the brighter arcs appear also without the application of a thermal gradient. The experiments were performed in 150 µm thick chambers with a solution of 200 mM dipotassium phosphate buffer, 3.2 mM supersaturated sodium myristate at pH 9.2 and 10 µM Cy5 labeled DNA.

enclosed by an outer ring, which marked the air bubble boundary at the cold side.[35] Light reflections in the right image

can easily be distinguished from high DNA concentrations, as they also occur for $\Delta T = 0\,K$ with $T = 24\,°C$, where the equilibrium prevents an accumulation of DNA. The overall drop in fluorescence intensity was attributed to the temperature dependence of the dye.

For the emergence of life, the localization of DNA at each foam bubble effectively generated an inverted cell structure. The gas bubbles evoke several microenvironments of accumulated DNA at each of the bubbles. They offer slightly different local environmental conditions, based on the uneven distribution of DNA and the molecule transport between the foam bubbles is enhanced by the capillary flow and free diffusion, offering a complex spatial reaction setting, especially when the foam would be formed inside more complex rock pores. Inside the gas bubble, continuous evaporation and dew recondensation of water led to bright spots when dew encountered the warm side and thus redissolved previously dried fluorescent DNA there. Uneven arrangement of gas bubbles can lead to unevenly distributed concentrations in foam (Figure S12).

DNA-rich droplets accumulate at foam

Interestingly, highly concentrated structures appeared at the foam interfaces when the DNA was labelled with Cy5 (Figure 4a). To investigate these DNA-rich droplets further, a series of experiments with different DNA sequences and dyes were executed. We used a solution with 10 µM fluorophore labelled DNA (see Table S1 for details), 3.2 mM supersaturated sodium myristate, 200 mM dipotassium phosphate buffer at pH 9.2. The chamber thickness was 150 µm and the thermal gradient amounted $\Delta T = 12\,K$ with $T_{warm} = 49\,°C$.

Cy5 labeled DNA showed liquid-liquid phase separated structures at the bubble interfaces. We observed this behavior for 14 nucleotide long and 84 nucleotides long Cy5 labeled DNA (Figure 4a, d). However, accumulation of 6-Fam labeled DNA at the gas bubble interface did not show a similar DNA-rich droplets (Figure 4b). Interestingly, an experiment with Cy5 dye without DNA, also gave rise to DNA-rich droplets at the gas bubble interfaces, indicating that the hydrophobic Cy5 dye as major driver of the effect, causing DNA-rich droplets in fatty acid solutions. Their resemblance to cellular structures could offer another level of complexity useful for localized prebiotic reactions.

We modified the DNA sample from Figure 4c by replacing Cy5 with 6-Fam and swapping the 6 bases next to the dye by poly G_6. While the 6-Fam labeled DNA without integrated poly G_6 did show uniform accumulation at the interface, poly G_6 modified, 6-Fam labeled DNA gave rise to cumulated DNA structures. Thus, adding G-rich tails altered DNA-rich droplets at the interfaces. Inferred from the location in Figure 4, the GGGGGG-induced droplets are located in the bulk fluid of the interface. Given the fact that polymerization in the wet state is strongly reduced in its yield, we do not expect that this is the cause of the prominence of G in the polymerization product. Moreover, the polymerization of G is also enhanced in the dry state, indicating other mechanism for its preference, possibly
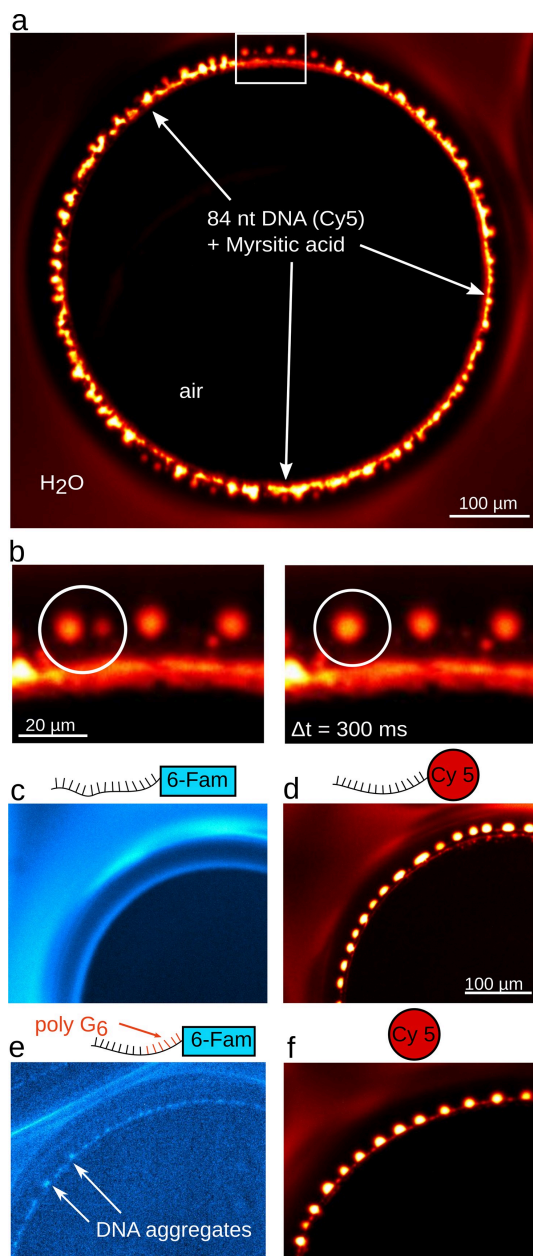
Figure 4. DNA-rich droplets form at heated foam interfaces. a) Cy5 labeled 84 nucleotide long DNA showed DNA-rich droplets at the accumulating, warm interface of gas bubbles (white arrows). b) Excerpt from white box (a), 300 ms apart. The DNA-rich droplets moved in the liquid phase at the warm interface, showing a fusion dynamic typical to oil droplets or coacervates. c, d) 6-Fam labeled 15 nucleotide long DNA did not show DNA-rich droplets while Cy5 labelled DNA of 14 nucleotides showed round structures, more homogeneous than the 84 nucleotide long DNA in (a). e) Replacing six bases of the 15 nucleotide long 6-Fam sequence by GGGGGG induced dot-like structures, indicating that the G-rich sequences also trigger the effect, confirming lipid interactions of G.[37] f) Only Cy5 dye as a sample showed uniform DNA-rich droplets at the interface as well. All experiments applied a thermal gradient of $\Delta T = T_{warm} - T_{cold} = 49\,°C - 37\,°C = 12$ K in 150 µm thick vessels. The sample consisted of 10 µM fluorescent DNA or dye (f), 200 mM dipotassium phosphate buffer and 3.2 mM sodium myristate.

due to the pK$_a$ of the base or its enhanced stacking interaction.[38]

The observed DNA-rich droplets were either stuck at the warm interface or moved freely close to the interface (see Movie S3). The freely moving DNA-rich droplets are recognizable by their isolated circular form. The structures touched and fused (Figure 4f), which is typical for coacervates studied in a thermal gradient before[39] or oil droplets.[40] We would characterize the droplet structures rather as coacervates than vesicles as we measured them to be 3 µm–7 µm in size and larger than vesicles, which are up to 100 nm in size.[41] Surfactants typically form micelles rather than vesicles.[33]

Accumulation of sequence dependent DNA aggregates

Sequence-dependent large scale DNA aggregates can be obtained from self-binding of ssDNA.[3,5,42–46] With the same experimental parameters as in Figure 4, a 36 nucleotide long 6-Fam labeled DNA sequence of G and C was designed to self-assemble into large DNA networks (Figure 5a). After the application of a thermal gradient ($\Delta T = 12$ K with $T_{warm} = 49\,°C$) the accumulation of DNA aggregates became visible within minutes (Figure 5b) and grew to larger, ring-like assemblies. Sequences which were not self-binding did not create comparably large aggregates as seen in Figure 3 and 4).
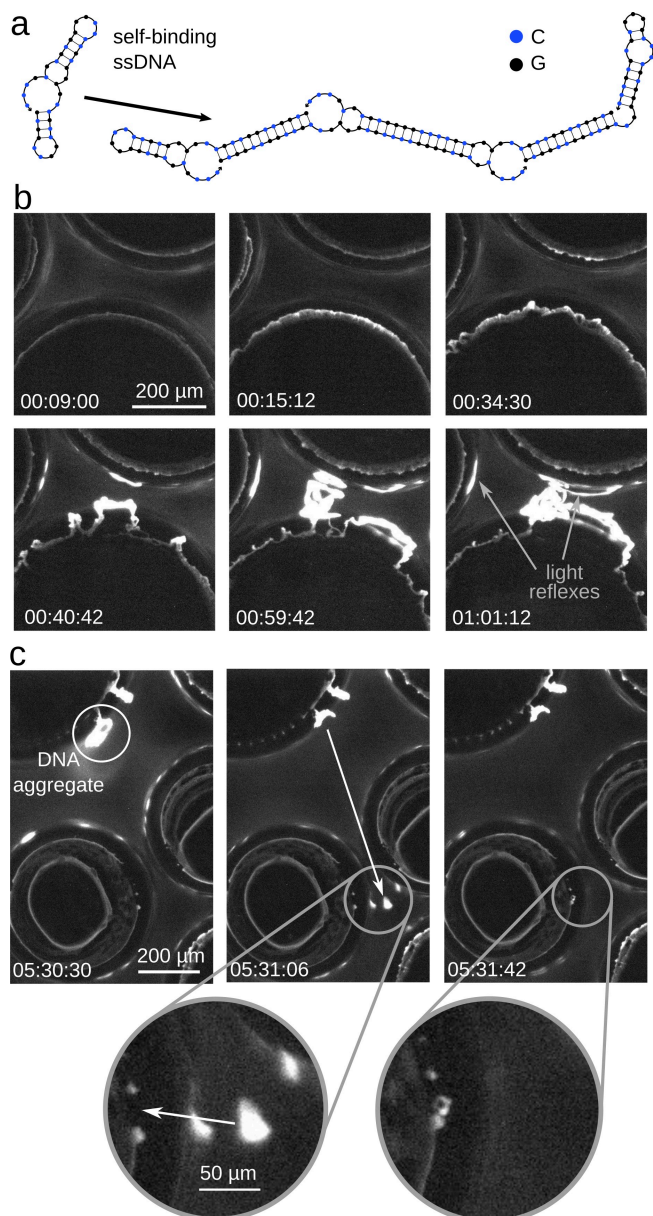
This sequence dependent accumulation by gel formation[3,25] gives RNA sequences a direct physical selection pressure: (i) the gel formation enhances the accumulation by the reduction in diffusion coefficient, making them more resistant to flow-based dilution away. (ii) The gelation enhances the formation of double stranded versus single stranded forms. This reduces the degradation of RNA by hydrolysis, leading to a sequence-dependent, multi-molecular selection pressure, adding a direct phenotype-genotype relationship for early Darwinian evolution.

The fluctuation of the gas bubble sizes caused sudden contractions of the gas-water interfaces, the aggregates could detach from one foam bubble and were transported by the capillary flows to another gas bubble (Figure 5c), demonstrating the sequence-dependent oligonucleotide transport in the foam. Compared to a single gas-water interface, foam offers more space for the formation of DNA aggregates[5] and the exchange between bubbles offers complex exchange modes for self-similar genetic material.

GC polymerization

Foams are particularly interesting for reactions relying on wet-dry cycles and as seen, already short oligonucleotides show very diverse selective phenotypes. To approach prebiotic scenarios, we therefore explored the effectiveness of the wet-dry cycles for the polymerization of short RNA from prebiotic more probable 2′,3′-cyclic nucleotides. Verlander et al. observed polyA oligomers up to a length of six nucleotides at alkaline pH conditions and temperatures from 20 °C to 70 °C with the help of amine catalysts.[27] Under such conditions a transesterification[47] of the phosphate group can occur, which results in the conversion of the 2′3′-cyclic phosphate group to a

ChemBioChem

Research Article
doi.org/10.1002/cbic.202200423

Chemistry
**Europe**
European Chemical
Societies Publishing

Figure 5. Aggregates of self-binding ssDNA form at the foam interfaces. a) Self-binding 36 nucleotide long ssDNA of G and C is designed to self-assemble into complex aggregates. b) Driven by a thermal gradient of $\Delta T = 12$ K with $T_{warm} = 49\,°C$, 10 µM 6-Fam labeled ssDNA is forming aggregates that grew over several minutes, gaining size through fluctuations of the gas-water Interface (Movie S4). c) Grown aggregates were detached from the interface and were transported through the bulk solution by diffusion and capillary flows. The circular excerpts show magnified images of the DNA aggregate docking at another bubble. The trap thickness was 150 µm. The solution included 3.2 mM sodium myristate and 200 mM dipotassium phosphate buffer.

3′,5′ or 2′,5′ linkage. In recent study, 2′,3′ cyclic nucleotides were shown to self-polymerize without catalysts under low salt conditions and elevated pH in the dry state. In case of mixed oligonucleotides polyG leads the copolymerization.[38] Therefore, the wet-dry cycling inherent to the heated foam was tested.

We compared the polymerization from cGMP and cCMP in foam to polymerization in a system with significantly lower

interfacial area. We could keep the conditions like before, using a solution of 3.6 mM sodium myristate, 200 mM phosphate buffer, 25 mM cGMP and 25 mM cCMP each and KOH to adapt the pH to pH 9.2. After 19.5 hours the pH of the extracted sample dropped to 8.6.

In Figure 6a, the resulting polymers were quantified by HPLC-ESI-TOF mass spectrometry measurements. The high surface to bulk ratio in the foams lead to higher concentrations of polymerization products compared to the non-foam counterpart. The reaction in foam has progressed further (up to 8mers) than in non-foam (up to 5mers). The chamber thickness and
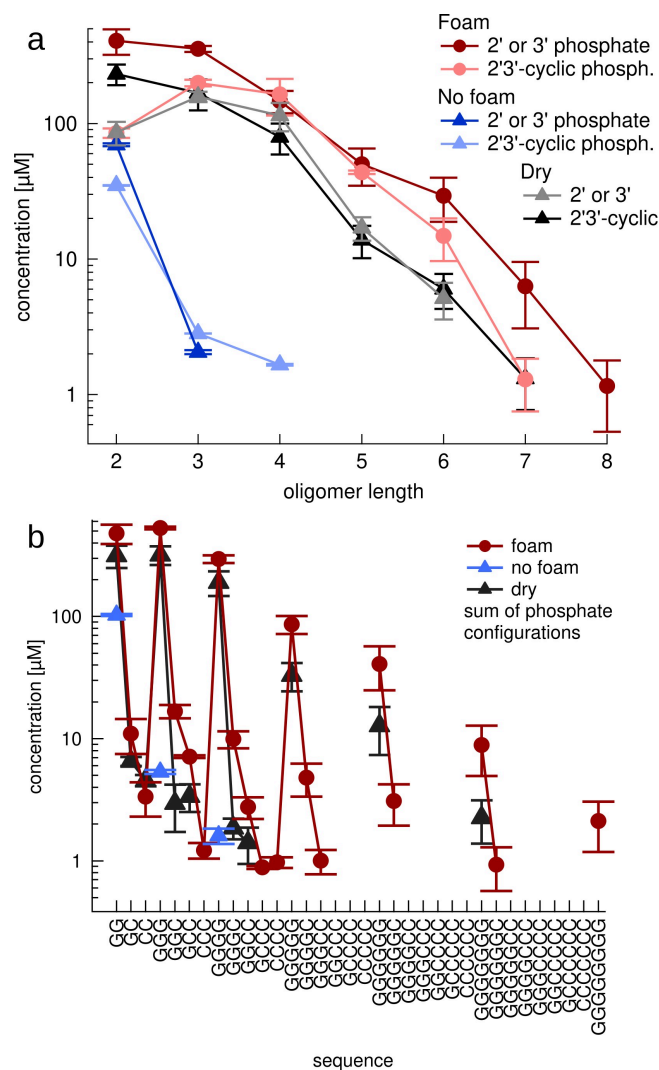
Figure 6. Foam induced polymerization of 2′,3′-cGMP and 2′,3′-cCMP. a) The wet-dry cycling conditions at the moving interfaces led to the oligomerization of RNA. The heated foam setting provided wet-dry cycles for polymerization (red), while a control experiments without bubbles did not oligomerize significantly (blue). The samples were exposed to a thermal gradient of $\Delta T = 25$ K with $T_{warm} = 59\,°C$ for $t = 19.5$ hours. When the whole solution was dried to T_{warm}, the oligomerization yield was significantly lower (grey) despite subjecting all nucleotides to the reactive dry condition. Oligomers with linear phosphate ends were found, indicating significant hydrolysis towards the unreactive, open ended monophosphates. b) The sequences detected by mass spectrometry showed sequences that integrated the less reactive C base, but also confirmed that longer oligonucleotides were dominated by polyG.

temperatures in the polymerization experiments were 500 μm, $T_{cold} = 34\,°C$ and $T_{warm} = 59\,°C$. In b the sequence space of the same experiment can be seen. The sequences that occur in both experiments are much higher concentrated in the foam experiment. Without foam, the maximum length of the resulting polymers was G_4, while polymerization in foam gave rise to G_8 at a higher concentration.

The foam brings together both the dry and wet state, offering increased flexibility for prebiotic reactions. It has been established previously that the oligomerization is driven in the dry state.[23–25,38] In the foam setting, only a small fraction of the molecules are in the dry state at the air-water interface on the warm side. One could therefore expect that the oligomerization in the foam should be less effective than when the whole solution would be dried. However the opposite is true. As reported in Figure 6 with the grey data points, the oligomerization in the fully dry condition is yields significantly less than for the reaction in the heated foam. At this point, we can only speculate that this might be due to the length dependent accumulation at the interface.[7,38,39]

It is important to note that the shown oligomerization is inefficient in comparison to polymerization reactions known in chemistry. But if prebiotic chemistry would have provided very efficient polymerization for RNA, any competing replicative mechanism would have been overwhelmed by a large amount of non-replicated, polymerized RNA, making Darwinian evolution a difficult past. However our results can be compared to previously reported results by Verlander and Orgel.[26,27] There, homo-oligomers of cAMP in the presence of 5-fold excess of ethane-1,2-diamine showed a yield of 0.81% for a 6mer of polyA after 40 days. Im comparison, we observed here ~0.12% for a 6mer of oligoG without added catalysts after less than a day in a mixed GC setting. Adding other catalysts such as imidazole or urea required temperatures up to 85 °C and offered lower yields.[26,27]

Clearly, the rather short mixed sequence oligomers reported are quite a bit away from the short oligomers required to for example run a templated ligation chain reaction. We hope that we will be able to better understand the degradation pathways of 2'3'-cyclic monomers with future experiments. But already at this stage, if an RNA world would operate with trimers, recently shown with a harder to reach triphosphate activation,[48] the documented oligomerization could be a good source of raw materials for replication while at the same time offering strand separation functionality by the air-water interface.[7]

Conclusion

For prebiotic reactions, heated liquid-gas interfaces offer dry and wet cycling conditions for the molecules that were attracted by the ensuing capillary flows. Here we maximized the surface to volume ratio by creating foams using prebiotic more probable lipids for stabilization. The result was an array of molecule-accumulating habitats for DNA or RNA that form an inverted cellular geometry.

Instead of insulating molecules by a bilayer, the molecules are concentrated at each bubble of the foam and are free to transfer between individual bubble habitats. At these interfaces, we found that the accumulation by the capillary flows triggered the formation of DNA-rich droplets and the sequence-dependent formation of large scale oligonucleotide aggregates, extending experiments at single air-water interfaces.[5,39] The open setting also allows for thermophoretic accumulation effects, such as the accumulation of ions to boost RNA polymerization catalysis.[49]

Since both accumulation and the formation of agglomerates and coacervation-like structures was triggered by oligonucleotides, it was intriguing to find that the heated foam was also capable to produce them by polymerizing RNA up to 8mers directly from the prebiotically more probable 2',3'-cyclic GMP and CMP. These combined findings show an interesting convergence of physical settings and chemical synthesis, establishing a new paradigm of compartmentalization for the selection, accumulation and oligomerization of informational polymers for early prebiotic evolution.

Experimental Section

Sample preparation: The reaction mixture was prepared by mixing 720 μL of the 5 mM supersaturated sodium myristate solution with 100 μL of a 2 M K2HPO4 solution, 50 μL of a 500 mM 2'3'cGMP solution, 500 mM 2'3'cCMP solution and 75 μL of RNAse-free water. The pH was adjusted at 9.2 by adding 5 μL of 1 M KOH solution, resulting in 3.6 mM sodium myristate, 200 mM dipotassium phosphate, 25 mM 2'3'cGMP and 25 mM 2'3'cCMP.

Precipitation protocol: To provide best reproducibility, a precipitation protocol that was shown not to change oligomer concentrations down to 2nt significantly was developed. To an aqueous solution of the oligonucleotide sample 2 μL of 100 mg/mL of glycogen and 1/10th volume 5 M ammonium acetate was added. After mixing, 2–3 volumes of cold 100% ethanol was added. The final solution was incubated at 4 °C overnight. After incubation, the sample was centrifuged at 4 °C for 30 min at 15000 rpm. The remaining supernatant was carefully discarded and 10 μL of cold 70% ethanol was added. The sample was centrifuged again at 4 °C for 30 minutes at 15000 rpm. The supernatant was removed, and the dried pellet dissolved in 40 μL RNAse-free water for HPLC analysis.

HPLC and mass spectrometry: The measurements were performed on Agilent G6230BA LC/TOF with G5654 A 1260 InfinityII bioinert HPLC using a an Agilent AdvanceBio Oligonucleotide (4.6×150 mm, 2.7 μm) column with a pressure rating of 600 bar, heated to 60 °C. Oligomers were analyzed in a water-methanol solvent system with solvent A consisting of 200 mM HFIP and 8 mM TEA in water and solvent B a 50:50 methanol-water mixed with solvent A. After an initial flow of 1% B for first 5 minutes, followed by a gradient of 1% up to 30% B in 22.5 minutes and a gradient from 30% to 40% B in the next 15 minutes at 1 mL/minute. The TOF Mass spectrometer Agilent 6125 is equipped with a dual AJS ESI ion source, set to a gas temperature of 325 °C, gas flow at 8 l/min, nebulizer at 45 psig, sheath gas temperature at 400 °C and sheath gas flow at 11 l/min. and run in negative mode. The samples were analyzed in

the negative ion mode. The scan source parameters were negative mode, Vcap = 3000 V, nozzle voltage at 2000 V, fragmentor at 175 V, Skimmer at 65 and octapoleRFpeak value of 750.

Fitting TOF-MS data with LabView program: Raw spectra of the mass spectrometry was converted with MSConvert to a MS1 or MZ5 format. The timing of the oligomers on the HPLC separation was determined with standards and to also determine the ionization efficiency. The raw mass spectra between each time bracket were integrated before fitting. Species of the polymers were defined and the isotope distribution calculated and used to fit the raw spectra before species of different charge are integrated and were converted to concentrations using the calibration from oligomer standards.

Thermal chamber and imaging: The thermal chamber was cooled by a water bath from the back and heated using 3D printer heating rods on the front side. The chamber was defined by Sapphire windows in between a the chamber geometry was defined by Teflon foil that was cut with a plotter (GRAPHTEC CE6000-40 Plus). An Arduino Mega 2560 was used to control temperature. The aluminum blocks and the backside sapphire provided openings for tubes or temperature sensors (Greisinger, GTH 1170). A heat camera (Seek Thermal, SQ-AAA) allowed temperature measurement on the front sapphire. The experiments were either monitored by a Canon90D camera with a 5× magnifying lens or a fluorescence microscope. Fluorescence imaging for Cy5 and 6-Fam was provided concurrently by an OptoSplit under LED illumination. Long distance 2×, 5× or 10× objectives were used in reflected light and imaged with a Stingray F145-B camera through a self-built fluorescence imaging setup using Thorlabs lens tube components.

Acknowledgements

Conflict of Interest

The authors declare no conflict of interest.

Data Availability Statement

The data that support the findings of this study are available in the supplementary material of this article.

[1] S. A. Benner, *Astrobiology* **2010**, *10*, 1021–1030.
[2] L. E. Orgel, *Crit. Rev. Biochem. Mol. Biol.* **2004**, *39*, 99–123.
[3] A. Kühnlein, S. A. Lanzmich, D. Braun, *eLife* **2021**, *10*, 10.7554/eLife.63431.
[4] D. Braun, A. Libchaber, *Phys. Biol.* **2004**, *1*, P1.
[5] M. Morasch, J. Liu, C. F. Dirscherl, A. Ianeselli, A. Kühnlein, K. Le Vay, P. Schwintek, S. Islam, M. K. Corpinot, B. Scheu, D. B. Dingwell, P. Schwille, H. Mutschler, M. W. Powner, C. B. Mast, D. Braun, *Nat. Chem.* **2019**, *11*, 779–788.
[6] N. T. Arndt, E. G. Nisbet, *Annu. Rev. Earth Planet. Sci.* **2012**, *40*, 521–549.
[7] A. Ianeselli, M. Atienza, P. W. Kudella, U. Gerland, C. B. Mast, D. Braun, *Nat. Phys.* **2022**, *18*, 579–585.
[8] A. Salditt, L. M. R. Keil, D. P. Horning, C. B. Mast, G. F. Joyce, D. Braun, *Phys. Rev. Lett.* **2020**, *125*, 048104.
[9] P. W. Kudella, K. Preißinger, M. Morasch, C. F. Dirscherl, D. Braun, A. Wixforth, C. Westerhausen, *Sci. Rep.* **2019**, *9*, 1–11.
[10] P. W. Kudella, A. V. Tkachenko, A. Salditt, S. Maslov, D. Braun, *Proc. Natl. Acad. Sci. USA* **2021**, *118*, e2018830118.
[11] N. Lane, W. F. Martin, *Cell* **2012**, *151*, 1406–1416.
[12] D. Deamer, *Life* **2021**, *11*, 134.
[13] E. I. Jiménez, C. Gibard, R. Krishnamurthy, *Angew. Chem. Int. Ed.* **2021**, *60*, 10775–10783.
[14] Z. Liu, L. F. Wu, J. Xu, C. Bonfio, D. A. Russell, J. D. Sutherland, *Nat. Chem.* **2020**, *12*, 3–10.
[15] H. J. Kim, S. A. Benner, *Astrobiology* **2021**, *21*, 298–306.
[16] M. W. Powner, B. Gerland, J. D. Sutherland, *Nature* **2009**, *459*, 239–242.
[17] Y. Yamagata, H. Inoue, K. Inomata, *Origins Life Evol. Biospheres* **1995**, *25*, 47–52.
[18] R. Breslow, *Acc. Chem. Res.* **1991**, *24*, 317–324.
[19] Y. Li, R. R. Breaker, *J. Am. Chem. Soc.* **1999**, *121*, 5364–5372.
[20] H. Peng, B. Latifi, S. Müller, A. Lupták, I. A. Chen, *RSC Chem. Biol.* **2021**, *2*, 1370–1383.
[21] A. M. Pyle, *Science* **1993**, *261*, 709–714.
[22] S. I. Nakano, D. M. Chadalavada, P. C. Bevilacqua, *Science* **2000**, *287*, 1493–1497.
[23] M. Morasch, C. B. Mast, J. K. Langer, P. Schilcher, D. Braun, *ChemBioChem* **2014**, *15*, 879–883.
[24] J. E. Šponer, J. Šponer, A. Giorgi, E. Di Mauro, S. Pino, G. Costanzo, *J. Phys. Chem. B* **2015**, *119*, 2979–2989.
[25] S. Wunnava, C. F. Dirscherl, J. Výravský, A. Kovařík, R. Matyášek, J. Šponer, D. Braun, J. E. Šponer, *Chem. Eur. J.* **2021**, *27*, 17581–17585.
[26] M. S. Verlander, L. E. Orgel, *J. Mol. Evol.* **1974**, *3*, 115–120.
[27] M. S. Verlander, R. Lohrmann, L. E. Orgel, *J. Mol. Evol.* **1973**, *2*, 303–316.
[28] S. A. Wilde, J. W. Valley, W. H. Peck, C. M. Graham, *Nature* **2001**, *409*, 175–178.
[29] A. Huerre, V. Miralles, M. C. Jullien, *Soft Matter* **2014**, *10*, 6888–6902.
[30] P. Marmottant, J. P. Raven, *Soft Matter* **2009**, *5*, 3385–3388.
[31] D. W. Deamer, J. Oro, *BioSystems* **1980**, *12*, 167–175.
[32] T. M. Mccollom, G. Ritter, B. R. T. Simoneit, *Origins Life Evol. Biospheres* **1999**, *29*, 153–166.
[33] J. N. Israelachvili, *Intermolecular and Surface Forces*, 3rd. ed., Elsevier, **2011**.
[34] J. D. Toner, D. C. Catling, *Proc. Natl. Acad. Sci. USA* **2020**, *117*, 883–888.
[35] A. Ianeselli, C. B. Mast, D. Braun, *Angew. Chem.* **2019**, *131*, 13289–13294; *Angew. Chem. Int. Ed.* **2019**, *58*, 13155–13160.
[36] J. Schmelzer, F. Schweitzer, **1987**, *12*, 255–270.
[37] T. Czerniak, J. P. Saenz, *Proc. Natl. Acad. Sci. USA* **2022**, *119*, e2119235119.
[38] A. V. Dass, S. Wunnava, J. Langlais, B. von der Esch, M. Krusche, L. Ufer, N. Chrisam, R. C. A. Dubini, F. Gartner, S. Angerpointner, C. F. Dirscherl, P. Rovó, C. B. Mast, J. Šponer, C. Ochsenfeld, E. Frey, D. Braun *ChemSystemsChem* **2022**, *4*, e202200026.
[39] A. Ianeselli, D. Tetiker, J. Stein, A. Kühnlein, C. B. Mast, D. Braun, T.-Y. Dora Tang, *Nat. Chem.* **2021**, 1–8.
[40] T. Banno, S. Miura, R. Kuroha, T. Toyota, *Langmuir* **2013**, *29*, 7689–7696.
[41] E. van der Pol, A. N. Böing, P. Harrison, A. Sturk, R. Nieuwland, *Pharmacol. Rev.* **2012**, *64*, 676–705.
[42] M. Morasch, D. Braun, C. B. Mast, *Angew. Chem.* **2016**, *128*, 6788–6791; *Angew. Chem. Int. Ed.* **2016**, *55*, 6676–6679.

[43] O. A. Saleh, B. J. Jeon, T. Liedl, *Proc. Natl. Acad. Sci. USA* **2020**, *117*, 16160–16166.

[44] B. J. Jeon, D. T. Nguyen, O. A. Saleh, *J. Phys. Chem. B* **2020**, *124*, 8888–8895.

[45] D. T. Nguyen, O. A. Saleh, *Soft Matter* **2017**, *13*, 5421–5427.

[46] D. T. Nguyen, B. J. Jeon, G. R. Abraham, O. A. Saleh, *Langmuir* **2019**, *35*, 14849–14854.

[47] J. Otera, *Chem. Rev.* **2002**, *93*, 1449–1470.

[48] J. Attwater, A. Raguram, A. S. Morgunov, E. Gianni, P. Holliger, *eLife* **2018**, 7.

[49] T. Matreux, K. LeVay, A. Schmid, P. Aikkila, L. Belohlavek, A. Z. Çalışkanoğlu, E. Salibi, A. Kühnlein, C. Springsklee, B. Scheu, D. B. Dingwell, D. Braun, H. Mutschler, C. B. Mast, *Nat. Chem.* **2021**, *13*, 1038–1045.